nature communications

Article

https://doi.org/10.1038/s41467-025-62776-w

Targeted degradation of cell surface proteins through endocytosis triggered by cell-penetrating peptide-small molecule conjugates

Received: 6 December 2023

Accepted: 30 July 2025

Published online: 14 August 2025

Check for updates

A list of authors and their affiliations appears at the end of the paper

Targeted degradation of membrane-associated proteins, which constitute a crucial class of drug targets implicated in diverse disease pathologies, has garnered considerable attention in chemical biology and drug discovery recently. Taking advantage of the endosomal entrapment of cell-penetrating peptides (CPPs) in delivering bioactive macromolecules, we successfully construct a CPP-based platform for specific degradation of cell surface proteins by conjugation of target protein-binding small molecules (SMs) with different CPPs, resulting in the formation of CPP-mediated lysosome-targeting chimeras (CPPTACs). Through the endo-lysosomal pathway, CPPTACs exhibit a remarkable ability to degrade clinically significant plasma membrane proteins, including PD-L1, CAIX, and CB_2R. In contrast to LYTACs and similar technologies, CPPTACs drive the degradation of targets in a manner independent of specific lysosome-shuttling receptors, thus providing a widely applicable strategy for plasma membrane protein degradation, regardless of the cell types. Additionally, simpler structural design and broader therapeutic window for CPPTACs are expected since CPPs-mediated endocytosis and lysosomal degradation do not necessitate the three-component binding model typically required by other heterobifunctional degraders. Overall, consisting of small molecules and biocompatible cell-penetrating peptides, CPPTACs developed in this study represent a simple, adaptable, and effective approach for selectively degrading cell surface proteins in various cellular contexts with potential for application in both biological research and therapeutic interventions.

Plasma membrane-associated proteins constitute a significant category of drug targets due to their accessibility at the cell surface, involvement in numerous crucial signaling pathways, and association with a diverse array of diseases[1,2]. In contrast to conventional drug discovery methods that primarily concentrate on inhibiting protein function, targeted protein degradation (TPD) strategies present the capability to directly modulate protein levels, thereby potentially offering a more efficacious approach for treating diseases associated with abnormal protein expression[3–6]. These strategies have demonstrated considerable potential in the field of drug discovery. The classical proteolysis-targeting chimeras (PROTACs) are heterobifunctional compounds that facilitate the ubiquitination and subsequent

e-mail: hc.li@siat.ac.cn; liang.chen@siat.ac.cn; lj.fang@siat.ac.cn

degradation of the target protein through the endogenous proteasome system, thereby confining their action to cytosolic proteins[7]. Recently, novel TPD technologies, such as LYTACs[8–10], MoDE-A[11], PROTABs[12], kineTACs[13], and others[14–26], have emerged to specifically target membrane proteins. In these technologies, engineered bifunctional degraders are designed to tether the target protein of interest (POI) to a specific lysosome-targeting receptor (LTR), thus facilitating the internalization and subsequent trafficking of the cell-surface POI to lysosomes for degradation. However, it should be noted that the expression of such a membrane LTR varies among different cell types and tissues, which limits the widespread application of these TPD technologies. Furthermore, the presence of "hook effect" in the three-component binding model significantly constrains the therapeutic window of bifunctional degraders of this nature, thus restricting their potential as pharmaceutical agents[27,28]. Consequently, there is a strong need to develop TPD technologies that are not reliant on specific LTRs for the degradation of membrane targets.

Cell-penetrating peptides (CPPs) have the ability to traverse cellular membranes and promote the effective internalization of diverse biomolecules, such as proteins, nucleic acids, and small molecules[29]. Numerous CPP variants, such as PEN (Penetratin), TAT (Trans-Activator of Transcription), R9 (nona-arginine), Transportan, MPG (Pep-1), among others, have been identified and employed for intracellular cargo delivery. Based on the characteristics of CPPs, including their length, concentration, and physicochemical properties, as well as the nature of the cargoes they are associated with, the penetration of CPP-cargo complexes into biological membranes occurs through diverse uptake mechanisms[30,31]. Typically, CPPs facilitate the delivery of bioactive macromolecules via endocytic pathways, resulting in the rapid accumulation of CPP-cargoes within endosomes following internalization. The successful delivery of therapeutic cargoes to their target sites, while evading lysosomal degradation, is a significant hurdle in CPPs-mediated drug delivery[32]. However, the entrapment of cargo within endosomes offers a strategic opportunity for the targeted degradation of membrane-associated proteins through CPP-induced endocytosis followed by lysosomal trafficking. In addition, it is generally believed that CPPs can trigger endocytosis in a manner independent of specific LTRs[29], thereby the development of CPPs-based TPD platform may provide a widely applicable strategy for plasma membrane protein degradation.

Herein, we present the development of CPP-mediated lysosome-targeting chimeras (CPPTACs) achieved through the conjugation of membrane-protein binding small molecules (SMs) with various CPPs. These CPPTACs exhibit the ability to bind to specific membrane targets and induce endocytosis, leading to the entrapment of internalized proteins within endosomal vesicles and their subsequent delivery to lysosomes for degradation. We demonstrate that CPPTACs can efficiently degrade a range of plasma membrane proteins, including PD-L1, CAIX, and CB_2R, independently of specific LTRs. As small molecule-based degraders devoid of the high-dose "hook effect", CPPTACs hold significant promise for applications in chemical biology and drug discovery (Fig. 1a).

Results

Design and construction of CPPTACs

CPPs are commonly distinguished by their elevated content of positively charged amino acids, such as arginine or lysine, and frequently exhibit an amphipathic character. This particular structural configuration enables their interaction with negatively charged constituents of the cell membrane, such as phospholipids and glycans. The mechanism and cellular uptake of CPPs are predominantly influenced by the specific sequence of the CPP and the size of the cargo it carries. It is generally believed that endocytosis serves as the predominant mechanism for CPPs in delivering bioactive macromolecules, particularly at low concentrations. And various CPPs can act as inducers of distinct endocytic pathways, including clathrin-mediated endocytosis (CME), fast endophilin-mediated endocytosis (FEME), caveolae-mediated endocytosis (Cav), clathrin-independent carrier (CLIC)/glycosylphosphatidylinositol-anchored protein enriched early endocytic compartment (GEEC) endocytosis, macropinocytosis and phagocytosis, according to the current understanding of endocytosis[33]. Considering the significant variations in cellular uptake and endocytic pathways observed across different CPPs, we synthesized four distinct CPPs in this study in order to evaluate their efficacy in promoting targeted protein degradation (Fig. 1b). To facilitate conjugation with small molecules, an alkyne group was introduced at the N-terminal of each peptide. Among these peptides, CPP1, CPP2, and CPP3 consist of the PEN, TAT and R9 sequence, respectively. Additionally, CPP4 is a fusion peptide that incorporates non-D-arginine as a cell-penetrating sequence and NPGY as a lysosome-sorting sequence, known to enhance the internalization and lysosomal targeting of antibodies and nanobodies[16,34].

To evaluate the effect of these four CPPs on endocytosis activity, we synthesized biotin-labeled CPPs (Biotin-CPP1-4) through the copper(I)-catalyzed alkyne-azide cycloaddition reaction between Biotin-Azide and CPP1-4, and employed these CPPTACs to investigate the cellular uptake and lysosomal delivery of NeutrAvidin Protein Dylight 650 (NAP-650), an extracellular biotin-binding protein (Supplementary Fig. 1a). Higher fluorescence was observed in cells co-incubated with NAP-650 and Biotin-CPP1-4 at a molar ratio of 1:2.5, as compared to cells treated with NAP-650 alone or with Biotin-Azide. The confocal images demonstrated that both Biotin-CPP1 and Biotin-CPP2 bearing PEN and TAT sequence, respectively, exhibited greater efficacy in promoting the internalization of NAP-650 compared to Biotin-CPP4 bearing nona-D-arginine and NPGY fusion sequence (Fig. 1c). Notably, Biotin-CPP3 bearing R9 sequence exhibited the lowest internalization activity among these peptides. These findings contrast with the internalization patterns observed for Rhodamine B (RhB, a commonly used fluorescent dye which is stable in acidic environment) labeled CPPs, where PhB-CPP3 and PhB-CPP4 displayed enhanced cell membrane penetration efficacy compared to RhB-CPP1 and RhB-CPP2 (Supplementary Figs. 1a, b). Furthermore, inhibiting the lysosomal proteolytic activity using chloroquine (CQ) or Bafilomycin A1 (BAF) resulted in a higher accumulation of NAP-650 in each group (Fig. 1c and Supplementary Figs. 1c–e), indicating that the internalized protein underwent gradual degradation within lysosomes.

Next, four endocytosis inhibitors, chlorpromazine (CPZ), nystatin, 7-keto-cholesterol (7-KC) and ethylisopropylamiloride (EIPA), were utilized to investigate the potential mechanism of endocytosis triggered by our designed CPPTACs[33,35]. Despite the off-target inhibition effects, these four inhibitors are generally used to block CME, Cav/CLIC, CLIC, and macropinocytosis, respectively[33]. As shown, the internalization of NAP-650 mediated by Biotin-CPP1 decreased dominantly in the presence of CPZ, supporting that CME is involved in CPP1-based CPPTACs (Fig. 1d and Supplementary Fig. 1f). In contrast, the internalization of NAP-650 mediated by Biotin-CPP2 appeared to be inhibited by both nystatin and 7-KC, suggesting that CLIC is the primary mechanism of action for CPP2-based CPPTACs (Fig. 1e and Supplementary Fig. 1g). Similar to Biotin-CPP1, the addition of CPZ hindered the uptake of NAP-650 mediated by Biotin-CPP4, implying that CME is engaged in CPP4-based CPPTACs (Supplementary Fig. 1h). To be noted, it is difficult to draw definite conclusions about the endocytic pathways of the CPPTACs due to the non-specific and cross-reactive nature of these endocytosis inhibitors employed in this study[33]. These findings demonstrate that both the efficiency of internalization and the pathway of endocytosis are contingent upon the specific sequence of CPPs employed in CPPTACs.

CPP1 and CPP2 were then selected for further studies due to their superior ability to induce endocytosis of extracellular proteins. Flow cytometry analysis was conducted with A549 cells incubated with NAP-

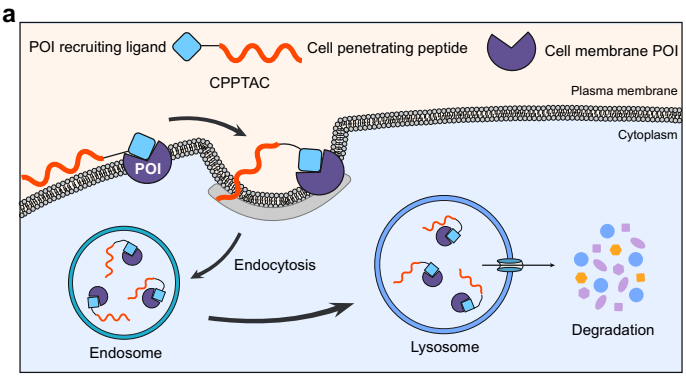

b

Peptide Sequences:

CPP1 (PEN): Alkyne-RQIKIWFQNRRMKWKK-NH_2

CPP2 (TAT): Alkyne-YGRKKRRQRRR-NH_2

CPP3 (R9): Alkyne-RRRRRRRRR-NH_2

CPP4 (CPP-LSS): Alkyne-GGrrrrrrrrrNPGY-NH_2

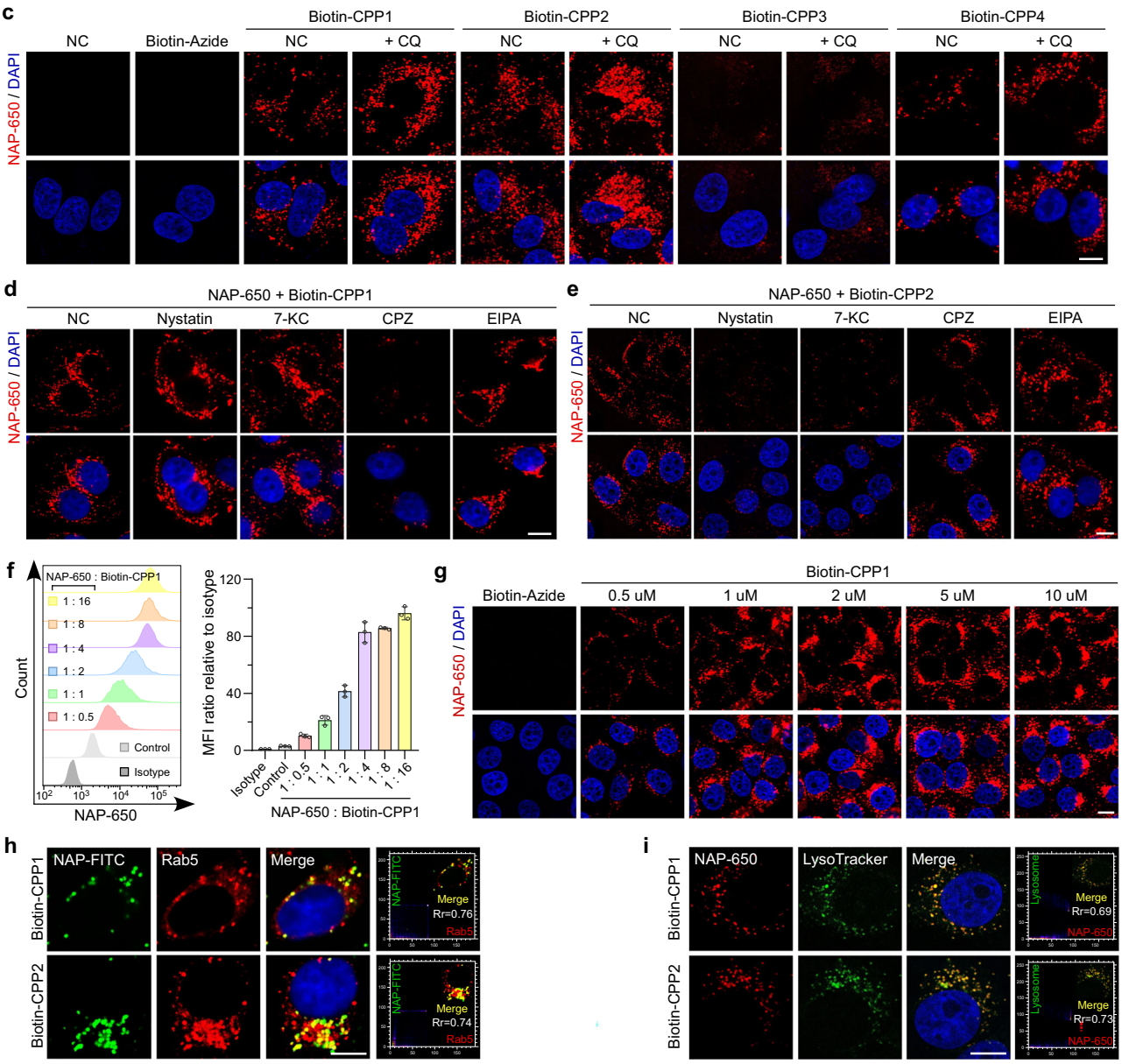

650 (0.5 μM) in combination with either Biotin-CPP1 or Biotin-CPP2 at specified molar ratios. As anticipated, a molar ratio of 1:4 facilitated better internalization compared to ratios of 1:0.5, 1:1, and 1:2. Increasing the molar ratio to 1:8 and 1:16 did not yield a significant enhancement in the internalization of NAP-650, as one NAP-650 molecule binds with four biotin molecules (Fig. 1f and Supplementary Fig. 2a, b). These findings are corroborated by results obtained through confocal laser scanning microscopy (CLSM) (Fig. 1g and Supplementary Fig. 2c). Additionally, a Trypan Blue quenching assay was conducted to remove proteins adhered to cell membranes during flow cytometry analysis[36]. Various concentrations of FITC-labeled NeutrAvidin protein (NAP-FITC) were utilized in place of NAP-650 because Trypan Blue does not have a quenching effect on Dylight 650. The results demonstrated only a minor reduction in fluorescence

Fig. 1 | CPPTACs promote the degradation of extracellular proteins through the endo-lysosomal pathway. a Schematic of the CPPTACs platform designed for targeted degradation of cell-surface proteins. **b** CPP1-4 with different peptide sequences. **c** Fluorescence analysis of the cellular uptake and lysosomal degradation of NAP-650 (red) mediated by different Biotin-CPP in A549 cells in the presence or absence of lysosomal proteolytic activity inhibitor, chloroquine (CQ). **d**, **e** Fluorescence analysis of the inhibitory effect of Nystatin (50 μM), 7-KC (7-ketocholesterol, 30 μM), CPZ (chlorpromazine, 10 μg/mL) or EIPA (ethylisopropylamiloride, 10 μg/mL) on the cellular uptake of NAP-650 (red) mediated by Biotin-CPP1 (**d**) or Biotin-CPP2 (**e**) in A549 cells. **f**, **g** Flow cytometry analysis (**f**) and fluorescence analysis (**g**) of the cellular uptake of NAP-650 (red) in A549 cells incubated with NAP-650 (0.5 μM) and Biotin-CPP1 at the indicated concentrations. Mean fluorescence intensity of NAP-650 relative to the untreated group was quantified ($n = 3$ biological replicates, means ± SD). **h** Fluorescence signals in A549 cells indicating the colocalization of NAP-FITC (green) with the early endosome marker (Rab5, red) mediated by Biotin-CPP1 or Biotin-CPP2. **i** Fluorescence signals in A549 cells indicating the colocalization of NAP-650 (red) with the lysosome marker (LysoTracker, green) mediated by Biotin-CPP1 or Biotin-CPP2. For **c**–**e**, **g**–**i**, the nuclei were labeled by DAPI (blue), scale bar, 10 μm. Source data are provided as a Source Data file.

signals in the Trypan Blue-treated groups compared to those without Trypan Blue treatment, suggesting that the fluorescence signals predominantly represent internalized NAP proteins rather than those attached to the cell membranes (Supplementary Fig. 2d, e). When co-incubated with Biotin-CPP1, the fluorescence signals of NAP-FITC co-localized with the early endosome marker (Rab5), and NAP-650 co-localized with lysosome marker (LysoTracker), supporting that the internalized proteins underwent trafficking through endosomes to lysosomes (Fig. 1h, i, and Supplementary Fig. 2f). Similar results were obtained when Biotin-CPP2 was employed, thereby demonstrating the capacity of CPPTACs to facilitate the internalization and lysosomal trafficking of extracellular proteins.

To verify whether the endocytosed protein mediated by CPPTACs can escape from endosomes or lysosomes, we employed a pH-sensitive fluorophore, naphthofluorescein (NF), as the reporter[37]. With a pKa value of ~7.8, NF is almost completely protonated and non-fluorescent (when excited at ≥590 nm) inside the endosomes or lysosomes (pH ≤ 6.0). Whilst a large increase in fluorescence intensity can be monitored once an NF-labeled CPP escapes from the endosome or lysosome into the cytosol, which typically has a pH of 7.4. For this purpose, NF-labeled CPPs, including NF-CPP1, NF-CPP2, and NF-Cyclic CPP (a well-established CPP known for its efficient endosomal escape capability[32]) were prepared along with the NF-labeled NeutrAvidin protein (NAP-NF) (Supplementary Fig. 2g). Among the compounds studied, NF-Cyclic CPP demonstrated a markedly higher fluorescence intensity relative to NF-CPP1 and NF-CPP2. Under identical imaging conditions, no fluorescence signals were detected in cells co-incubated with NAP-NF and Biotin-CPP1/Biotin-CPP2. These observations indicate that the target protein internalized through CPPTACs is largely unable to escape from endosomal or lysosomal compartments (Supplementary Fig. 2h).

Although the LTR-independent endocytosis has been frequently suggested for the majority of known CPPs, this mechanism lacks critical experimental validation. Therefore, we conducted a pooled CRISPR knockout (KO) screen to identify candidate receptors whose disruption would impede CPPTAC-mediated endocytosis of the targeted protein[8,10]. HeLa cells were initially transduced with a genome-wide CRISPR-Cas9 knockout (GeCKO) library, encompassing 19,686 genes targeted by 61,058 unique guide sequences. The cells were subsequently incubated with a mixture of Biotin-CPP1 and NAP-650. Fluorescence-activated cell sorting (FACS) was employed to isolate cells exhibiting a marked reduction in NAP-650 uptake. These cells were then subjected to high-throughput sequencing to identify the corresponding single guide RNAs (sgRNAs). The genes targeted by these sgRNAs are hypothesized to play a critical role in CPP1-mediated endocytosis (Fig. 2a). Our experimental findings indicate that no typical receptors are implicated in this process. Instead, genes associated with the regulation of glycosaminoglycan biosynthesis, heparin biosynthesis, and heparan sulfate proteoglycan biosynthetic process were identified as the top candidates, suggesting that heparin and other glycans are probably crucial mediators for CPP1-driven endocytosis (Fig. 2b, c)[38,39]. Mechanistically, these glycans possess substantial negative charges, which facilitate their binding to cationic CPPs, thereby promoting stable CPP association and subsequent endocytosis. To evaluate this hypothesis, a competitive binding experiment was performed utilizing 10-kDa branched polyethylenimine (PEI-B10k), a material with a high density of positive charges, to interact with the negatively charged constituents of the cell membrane. As expected, the introduction of PEI-B10k resulted in a decreased internalization of NAP-650 mediated by either CPP1- or CPP2-based CPPTAC (Fig. 2d, e). Additionally, the presence of heparin-Na, which is capable of interacting with the positively charged CPPs, also inhibited the uptake of NAP-650 mediated by CPP1/CPP2-based CPPTAC (Fig. 2f, g). Moreover, the efficient uptake of NAP-650 facilitated by Bioin-CPP1 was observed across a range of cell lines, with variations potentially attributable to differences in cell size or the presence of proteoglycans on the cell surface (Supplementary Fig. 2i). These observations suggest that the mechanism of action for CPPTACs is reliant on electrostatic interactions with negatively charged proteoglycans that are ubiquitously present on the surfaces of various cell types. Although receptors are not entirely excluded from CPPTAC-mediated endocytosis, our comprehensive genomic screening suggests that they are not significant regulators of this process.

Development of CPPTACs as PD-L1 degraders

Subsequently, we aimed to employ the CPPTACs approach to degrade plasma membrane proteins. As a proof of concept, we first targeted programmed death-ligand 1 (PD-L1), an essential immune checkpoint that is overexpressed in numerous tumor cells[40]. To achieve this, we synthesized BMS-CPP1 and BMS-CPP2 through covalent conjugation of CPP1/CPP2 with BMS-8, a small molecule known for its high binding affinity to PD-L1 (Supplementary Fig. 3a)[41]. To examine the potential degradation ability of these CPPTACs on cell-surface PD-L1, MDA-MB-231 cells were treated with BMS-CPP1 and BMS-CPP2, respectively, and the level of PD-L1 was evaluated. As shown, both BMS-CPP1 and BMS-CPP2 caused rapid degradation of PD-L1, with 65-75% degraded within 8 h and this degradation lasted for 24 h. Furthermore, BMS-CPP1 exhibited superior degradation efficiency compared to BMS-CPP2 across the concentration range of 5 nM to 250 nM, with maximum degradation rates of approximately 75% and 65% respectively (Fig. 3a, b). Significantly, neither BMS-CPP1 nor BMS-CPP2 exhibited the 'hook effect', a characteristic observed in classical heterobifunctional chimeras that rely on a three-component binding model, suggesting that these CPPTACs possess a wider concentration window as membrane protein degraders. At equivalent concentration (50 nM), BMS-CPP1 demonstrated a slightly higher performance compared to PD-LYSO, a rationally designed peptide incorporating the lysosome-sorting signal and the PD-L1-binding sequence of HIP1R (Fig. 3c, d)[42]. In addition, treatment with either BMS-CPP1 or BMS-CPP2 resulted in a substantial decrease of 75-80% in PD-L1 levels in HeLa cells stably expressing HA-PD-L1 (HeLa-HA-PD-L1 cells) (Fig. 3e). In contrast, the treatment of MDA-MB-231 cells with 5-250 nM of BMS-8 for 8 h resulted in an apparent increase in PD-L1 expression, rather than its degradation (Supplementary Fig. 3b)[43]. And minimal changes in PD-L1 levels were observed in HeLa-HA-PD-L1 cells treated with BMS-8 within the concentration range of 5 to 250 nM (Supplementary Fig. 3c). Accordingly, immunofluorescent microscopy revealed a remarkable reduction of surface HA-PD-L1 in cells treated with BMS-CPP1, whereas less impact

https://doi.org/10.1038/s41467-025-62776-w

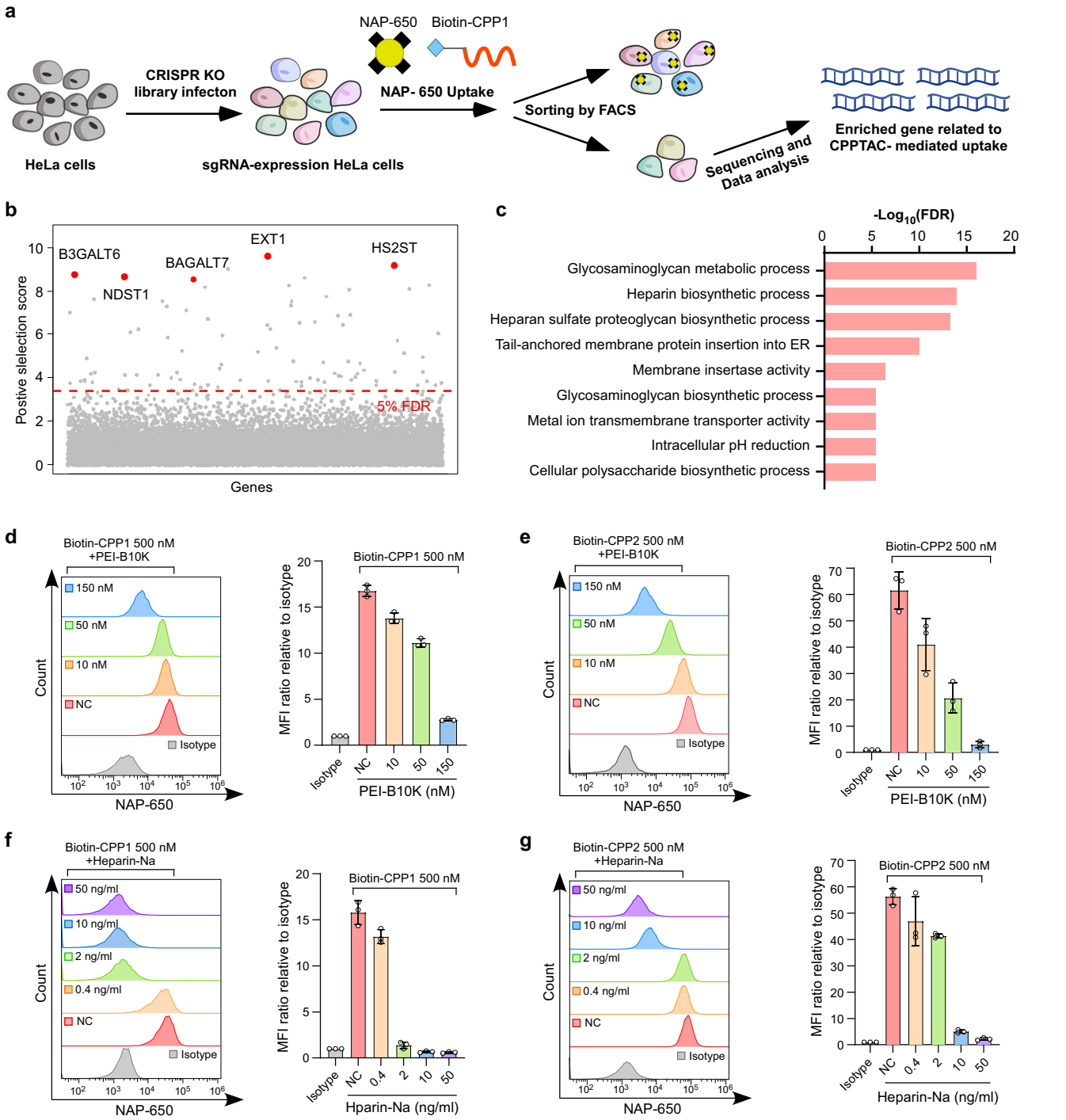

Fig. 2 | CPPTACs mediate the internalization of extracellular proteins independently of specific lysosome-targeting receptors (LTRs). a The schematic of CRISPR KO screen in HeLa cells transduced with a genome-wide CRISPR-Cas9 knockout library targeting 19,686 genes. **b** Selected gene hits for regulation of NAP-650 internalization by Biotin-CPP1. **c** Top GO terms enriched in significant hits (<5% FDR) from positive selection. **d**, **e**, **f**, **g** Flow cytometry analysis of the inhibitory effect of PEI-B10K or Heparin-Na at the indicated concentrations on the cellular uptake of NAP-650 (100 nM) mediated by Biotin-CPP1 (500 nM) (**d**, **f**) or Biotin-CPP2 (**e**, **g**) in HeLa cells. Mean fluorescence intensity of NAP-650 relative to the untreated group was quantified ($n = 3$ biological replicates, means ± SD). Source data are provided as a Source Data file.

was observed when BMS-8, CPP1, or a combination of both were utilized, thereby excluding the influence of the protein-binding molecule and the cell-penetrating peptide themselves (Fig. 3f). In comparison to the significant reduction of the plasma membrane protein, HA-PD-L1 situated in the cytoplasm exhibited minimal impact following exposure to BMS-CPP1 (Fig. 3g). This selective degradation may account for the observed inability of CPPTACs to induce complete protein degradation. The degradation effect of BMS-CPP1 on PD-L1 was similarly observed in U87-MG, NCI-H1975 and NCI-H292 cells, indicating the broad applicability of CPPTACs across different cell types (Fig. 3h). Furthermore, the fluorescence signals of RhB-BMS-CPP1 (RhB labeled BMS-CPP1) were markedly higher in HeLa-HA-PD-L1 cells compared to HeLa cells with low PD-L1 expression, suggesting that the internalization of RhB-BMS-CPP1 is dependent on the expression levels of cell

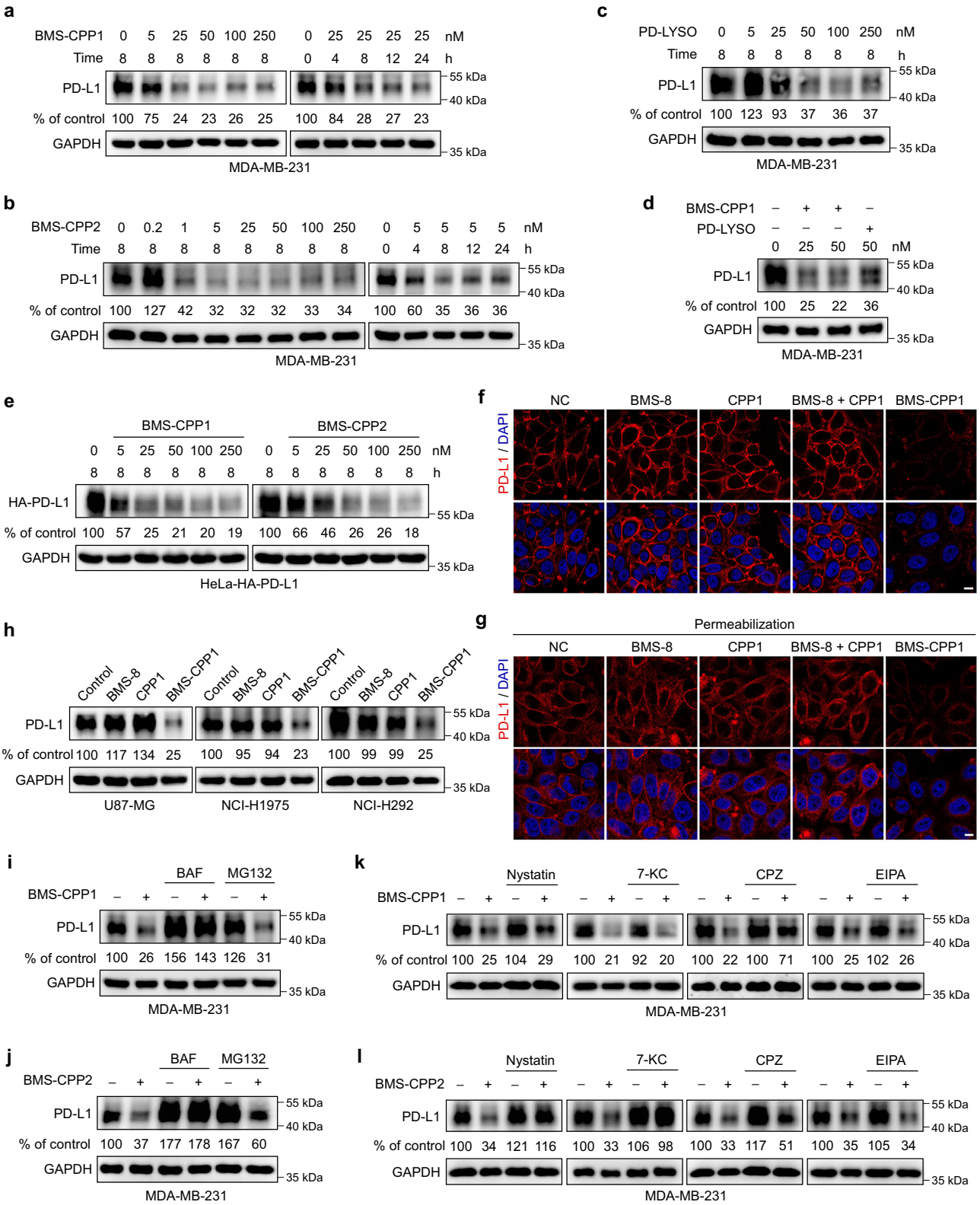

surface PD-L1 at the tested concentrations (5-100 nM) (Supplementary Figs. 3d, e).

To confirm that CPPTACs-mediated PD-L1 degradation was progressed through endo-lysosomal pathway, we investigated the degradation performance of BMS-CPP1 and BMS-CPP2 in cells that were pretreated with a lysosome inhibitor (BAF) and a proteasome inhibitor (MG132), respectively. As expected, BAF treatment, but not MG132 treatment resulted in a visible reduction of PD-L1 degradation (Fig. 3i, j). These findings demonstrate that CPPTACs-mediated degradation is reliant on the lysosomal pathway. Consistent with the uptake of extracellular protein, the degradation of surface PD-L1 mediated by CPP1-based CPPTAC primarily relied on CME endocytosis, while CPP2-based CPPTAC predominantly drove PD-L1 degradation through CLIC endocytosis (Fig. 3k, l), suggesting the possibility of employing different endocytic pathways in this CPPTACs platform. In addition, the existence of Galectin-9 (Gal9) recruitment, a reporter for membrane

Fig. 3 | CPPTACs drive the degradation of PD-L1 through the endo-lysosomal pathway. a, **b** Western blot analysis of PD-L1 levels in MDA-MB-231 cells treated with BMS-CPP1 (**a**) or BMS-CPP2 (**b**) at indicated concentration, or indicated time. **c**, **d** Western blot analysis of PD-L1 levels in MDA-MB-231 cells treated with PD-LYSO (**c**, **d**) or BMS-CPP1 (**d**) for 8 h at indicated concentration. **e** Western blot analysis of HA-PD-L1 levels in HeLa cells (stably expressing HA-PD-L1) treated with BMS-CPP1 or BMS-CPP2 for 8 h at indicated concentration. **f**, **g** Immunofluorescence analysis of PD-L1 (red) degradation on cell membrane (**f**) or in whole cells (**g**). HeLa cells stably expressing PD-L1 were treated with BMS-CPP1, BMS-8, CPP1, or a combination of BMS-8 and CPP1. The nuclei were labeled by DAPI (blue). Scale bar, 10 μm. **h** Western blot analysis of PD-L1 levels in different cell lines treated with 25 nM of BMS-CPP1, BMS-8 or CPP1 for 8 h. **i**, **j** Western blot analysis of PD-L1 levels in MDA-MB-231 cells treated with 25 nM of BMS-CPP1 (**i**) or 5 nM of BMS-CPP2 (**j**) for 8 h along with bafilomycin A1 (100 μM) or MG132 (5 μM). **k**, **l** Western blot analysis of the inhibitory effect of Nystatin (50 μM), 7-KC (7-keto-cholesterol, 30 μM), CPZ (chlorpromazine, 10 μg/mL) or EIPA (ethylisopropylamiloride, 10 μg/mL) on the degradation of PD-L1 mediated by BMS-CPP1 (**k**) or BMS-CPP2 (**l**). Source data are provided as a Source Data file.

damages[44], was not observed in Hela-PD-L1-bla GFP-Gal9 cells upon treatment with BMS-CPP1 or BMS-CPP2, suggesting that evasion of the endocytosed CPPTACs and the target protein did not occur through disruption of endosomal or lysosomal membrane integrity (Supplementary Fig. 3f). Collectively, these findings indicate that CPPTACs, comprised of small molecules and CPPs bearing diverse peptide sequences, have the capacity to effectively induce the targeted degradation of plasma membrane proteins through the endo-lysosomal pathway.

Considering that the lengths of the linker utilized to connect CPPs and POI recruiting SMs may have an influence on the degradation efficacy of CPPTACs, we synthesized BMS-L2-CPP1 and BMS-L3-CPP1, incorporating longer linker lengths, and assessed their effectiveness in promoting PD-L1 degradation in comparison to BMS-CPP1 (structurally equivalent to BMS-L1-CPP1) (Supplementary Fig 3g). As expected, both BMS-L2-CPP1 and BMS-L3-CPP1 exhibited good degradation activity in MDA-MB-231 cells at a concentration as low as 5 nM, resulting in a similar reduction (70-75%) of PD-L1 levels compared to BMS-CPP1 (Supplementary Fig. 3h). Furthermore, neither BMS-L2-CPP1 nor BMS-L3-CPP1 exhibited a 'hook effect' within the concentration range of 5 nM to 250 nM. These findings demonstrate that CPPTACs possess a high tolerance for both linker lengths and working concentrations, thereby offering convenience in the design and utilization of such degraders.

Given the demonstrated ability of CPPTACs to degrade PD-L1 in tumor cells, we proceeded to assess the in vivo antitumor effects of BMS-CPP1 using the B16F10 tumor xenograft C57BL/6 J mouse model (Fig. 4a). Tumor-bearing mice were administered BMS-CPP1 (10 mg/kg), BMS-8 (2 mg/kg), or CPP1 (4 mg/kg) via intravenous injection every 2 days. Throughout the treatment period, CPP1 displayed slight toxicity, leading to noticeable weight losses, while no side effects were observed in the other groups. And the differences in body weight between the BMS-CPP1/BMS-8 treated group and the control group were likely due to variations in tumor sizes (Fig. 4b). As anticipated, the tumor growth of BMS-CPP1 treated mice was significantly suppressed in comparison to the other experimental groups (Fig. 4c). At the end of treatment, the tumors were excised and weighed (Fig. 4d, e). As shown, BMS-CPP1 displayed improved efficacy in inhibiting tumor growth relative to BMS-8 and the combined administration of BMS-8 (1 mg/kg) and CPP1 (2 mg/kg) (Supplementary Figs. 4a–e). Additionally, a reduced incidence of metastasis was observed in the spleen of the BMS-CPP1-treated mice, suggesting a potential role for BMS-CPP1 in metastasis inhibition (Fig. 4f). Although BMS-8 exhibited some inhibitory effects on tumor growth, the PD-L1 level in BMS-8-treated group were similar to that in the control group, suggesting that BMS-8 alone did not promote PD-L1 degradation (Fig. 4g). Furthermore, immunohistochemical analysis of tumor tissues also revealed a significant decrease of PD-L1 in the BMS-CPP1-treated group relative to both the BMS-8-treated group and other groups (Fig. 4h). Subsequent experiments showed that two doses of BMS-CPP1 resulted in a remarkable reduction in PD-L1 levels in tumor tissues (Supplementary Figs. 4f–h). These observations suggest that BMS-CPP1 and BMS-8 inhibit PD-L1 function via distinct mechanisms of action. By removing PD-L1 from the cell surface, BMS-CPP1 may potentially address the drug resistance challenges commonly associated with small-molecule inhibitors targeting PD-L1. Additionally, Cy5.5-BMS-CPP1 (Cy5.5-labeled BMS-CPP1) exhibited enhanced tumor accumulation and reduced distribution in non-target organs such as the liver, spleen, lung, and kidney, relative to Cy5.5-CPP1 (Cy5.5-labeled CPP1). Notably, the liver displayed significantly elevated fluorescence signals compared to other organs, indicating that both Cy5.5-CPP1 and Cy5.5-BMS-CPP1 are predominantly metabolized through hepatic pathways (Supplementary Figs. 4i–l). Collectively, our findings demonstrate that the newly developed CPPTAC, BMS-CPP1, has the ability to degrade PD-L1 in vivo, leading to significant tumor suppression effects in mice with minimal side effects, thus providing new opportunities for anticancer drug discovery[40].

Expansion of the Target Scope of CPPTACs

After confirming the efficacy of CPPTACs in vitro and in vivo for the elimination of PD-L1, our study aimed to extend the utilization of this approach to degrade additional plasma membrane proteins. Carbonic anhydrase IX (CAIX), a transmembrane metalloenzyme, is known to be overexpressed in aggressive and invasive tumors[45]. It plays a crucial role in catalyzing the conversion of carbon dioxide hydrates into bicarbonate and protons, thus creating a favorable pH environment for the survival and growth of tumor cells within an acidic microenvironment. Multiple studies have demonstrated that the inhibition of CAIX function through the use of small molecule inhibitors effectively suppressed tumor growth and metastasis[46]. Therefore, we intended to develop CPPTACs that possess the ability to specifically target and degrade CAIX. To construct CAIX degraders, we selected 4, 4-[5-(aminosulfonyl)-1,3,4-thiadiazole] amino]-4-oxobutyric acid (Sul-acid) due to its high affinity for CAIX[47], and conjugated it with CPP1 and CPP2, resulting in the formation of Sul-CPP1 and Sul-CPP2 respectively (Fig. 5a). In accordance with the degradation of PD-L1 mediated by CPPTACs, the administration of Sul-CPP1 or Sul-CPP2 led to a rapid decline of CAIX in MDA-MB-231 cells. A significant reduction (75-80%) of CAIX was observed after 4-hour incubation of the cells with Sul-CPP1 and Sul-CPP2 at concentrations of 25 nM and 50 nM, respectively (Supplementary Fig. 5a, b). Furthermore, the presence of the "anti-hook effect" was demonstrated as the augmentation of Sul-CPP1 and Sul-CPP2 concentrations exerted negligible influence on their degradation activity (Fig. 5b, c). The degradation effect was attributed to the Sul-CPP1 conjugate, since neither Sul-acid nor CPP1 treatment elicited an obvious reduction in CAIX (Fig. 5d). Additionally, the degradation of CAIX was found to occur through the endo-lysosomal pathway, as evidenced by its restoration following treatment with the lysosome inhibitor bafilomycin A1 (Fig. 5e). The inhibitory effect of CPZ on the degradation of CAIX mediated by Sul-CPP1 confirms the predominant role of CPP1-based CPPTACs in stimulating CME endocytosis (Fig. 5f). Conversely, the inhibition of Sul-CPP2-mediated degradation by both nystatin and 7-KC provides evidence for the primary involvement of CPP2-based CPPTACs in promoting CLIC endocytosis (Fig. 5g). Altogether, these results suggest that the degradation of cell surface enzymes can be achieved through utilization of CPPTACs. Furthermore, the endocytic pathway of various CPPTACs is determined by the specific peptide sequences employed, rather than being influenced by the POI target.

Meanwhile, we investigated the impact of Sul-CPP1 on tumor cells under a hypoxic microenvironment induced by cobalt

https://doi.org/10.1038/s41467-025-62776-w

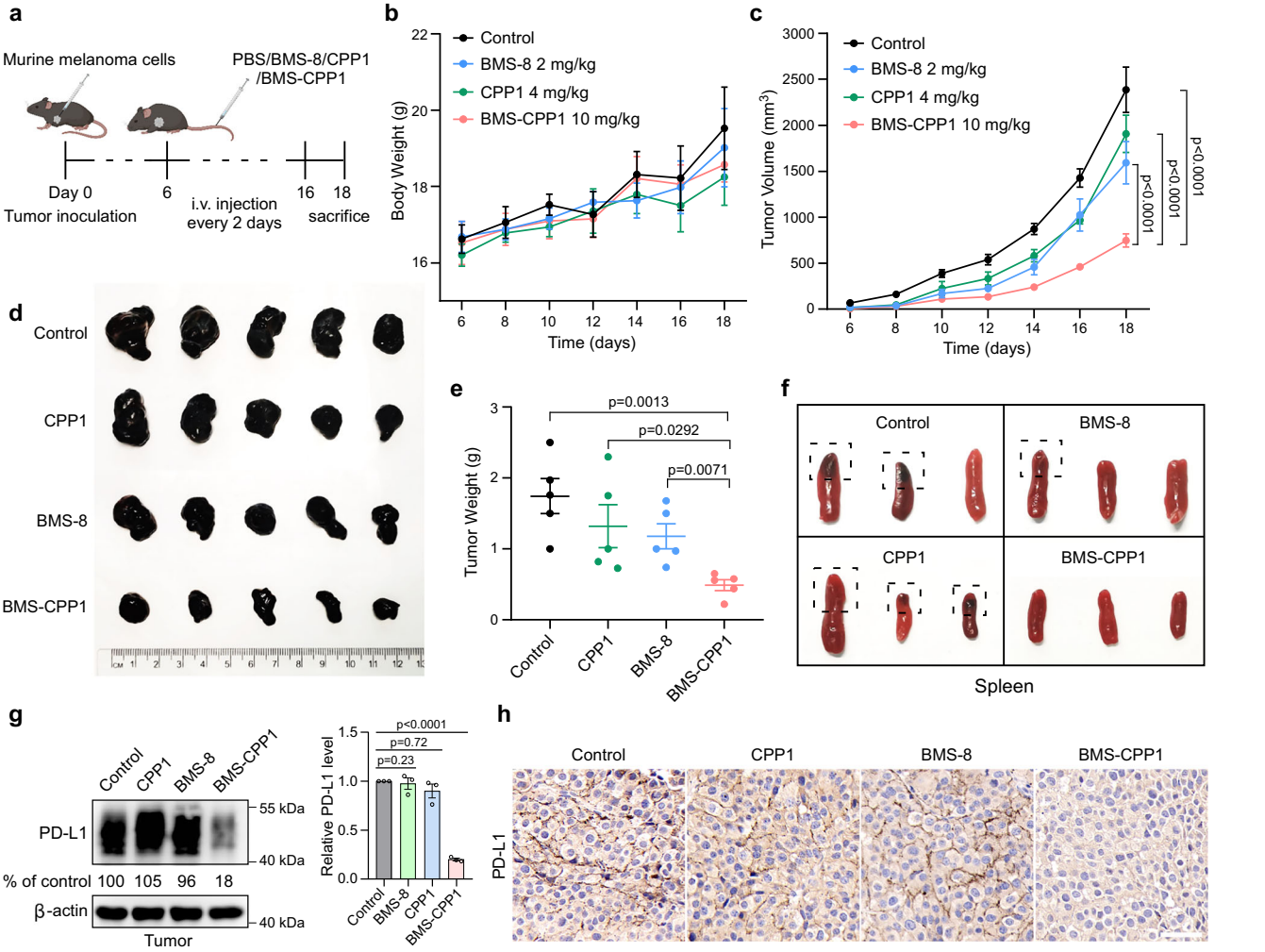

Fig. 4 | CPPTAC (BMS-CPP1) exhibits antitumor efficacy in vivo through facilitating the degradation of PD-L1. a Schematic illustration of the tumor-inhibition study and the general treatment procedure. Created in BioRender. OU, ZI. (2025) https://BioRender.com/8m9xnsp. **b** Body weight change curves of mice from day 6 to day 18. Data represent the mean ± SEM ($n = 5$ mice per group). **c** Tumor growth curves for each group. Comparison of the tumor size after 18 days of different treatments. Data represent the mean ± SEM ($n = 5$ mice per group). The statistical significance was assessed using two-way ANOVA. **d** Photograph of the peeled-off tumors of all four groups. **e** Comparison of the tumor weight after tumor dissection. Data represent the mean ± SEM ($n = 5$ mice per group). The statistical significance was assessed using two-tailed Student's *t*-tests. **f** Metastasis of tumor in the spleens of each group. **g** Western blot analysis of PD-L1 in B16F10 tumor tissues. Densitometry was used to calculate protein levels, and data were normalized to control. Data represent the mean ± SEM ($n = 3$ mice per group). Statistical significance was assessed using two-tailed Student's *t*-tests. **h** Representative immunohistochemical staining of PD-L1 in tumor tissues. Scale bar, 50 μm. Source data are provided as a Source Data file.

dichloride ($CoCl_2$)[48]. Both western blot and flow cytometric analysis revealed an up-regulation of CAIX expression in MDA-MB-231 cells upon $CoCl_2$ treatment, while co-incubation with Sul-CPP1 resulted in a significant reduction of the cell surface CAIX (Fig. 5h and Supplementary Fig. 5c). Accordingly, significant inhibition of the tumor cell survival under hypoxic conditions induced by $CoCl_2$ was achieved upon Sul-CPP1 treatment, as determined by the CCK8 assay (Fig. 5i). Sul-CPP1 displayed a noteworthy capacity to suppress tumor cell viability, comparable to that of SLC-0111, a CAIX inhibitor currently being evaluated in clinical trials[49]. Meanwhile, the administration of Sul-acid and CPP1, either individually or in combination, only resulted in a minor impact on the survival of cancer cells in hypoxic conditions (Fig. 5j). These findings underscore the potential of CPPTACs as an effective strategy for the development of CAIX degraders with therapeutic applications.

Finally, our attention was directed towards the advancement of CPPTACs for the specific degradation of the cannabinoid type 2 receptor (CB_2R). CB_2R, classified as a class A G-protein-coupled receptor (GPCR), predominantly located in the immune system, as well as in microglia cells and neurons. Given its implication in diverse pathological states, CB_2R is increasingly recognized as a promising therapeutic target for addressing tissue damage, inflammation, and various neurodegenerative ailments[50]. While numerous structurally diverse CB_2R agonists have demonstrated encouraging outcomes in animal models, none have achieved clinical success thus far. Therefore, the development of CB_2R degraders is of great importance, as it would provide valuable biological tools to better understand the role of CB_2R in disease pathology. Accordingly, a CPPTAC (referred to as HU-CPP1) was constructed by the linkage of CPP1 to a HU-308 derivative (HU) that exhibits a strong affinity for CB_2R and a favorable selectivity towards CB_1R (Fig. 5k)[51]. The effectiveness of HU-CPP1 in degrading CB_2R was subsequently assessed in MDA-MB-231 and HT-29 cancer cell lines, as well as BV2 mouse microglia cell line. As anticipated, HU-CPP1 demonstrated a notable efficacy in promoting the degradation of CB_2R (70-75% reduction) with the "anti-hook effect" in the concentration range of 25 nM to 1000 nM, while almost

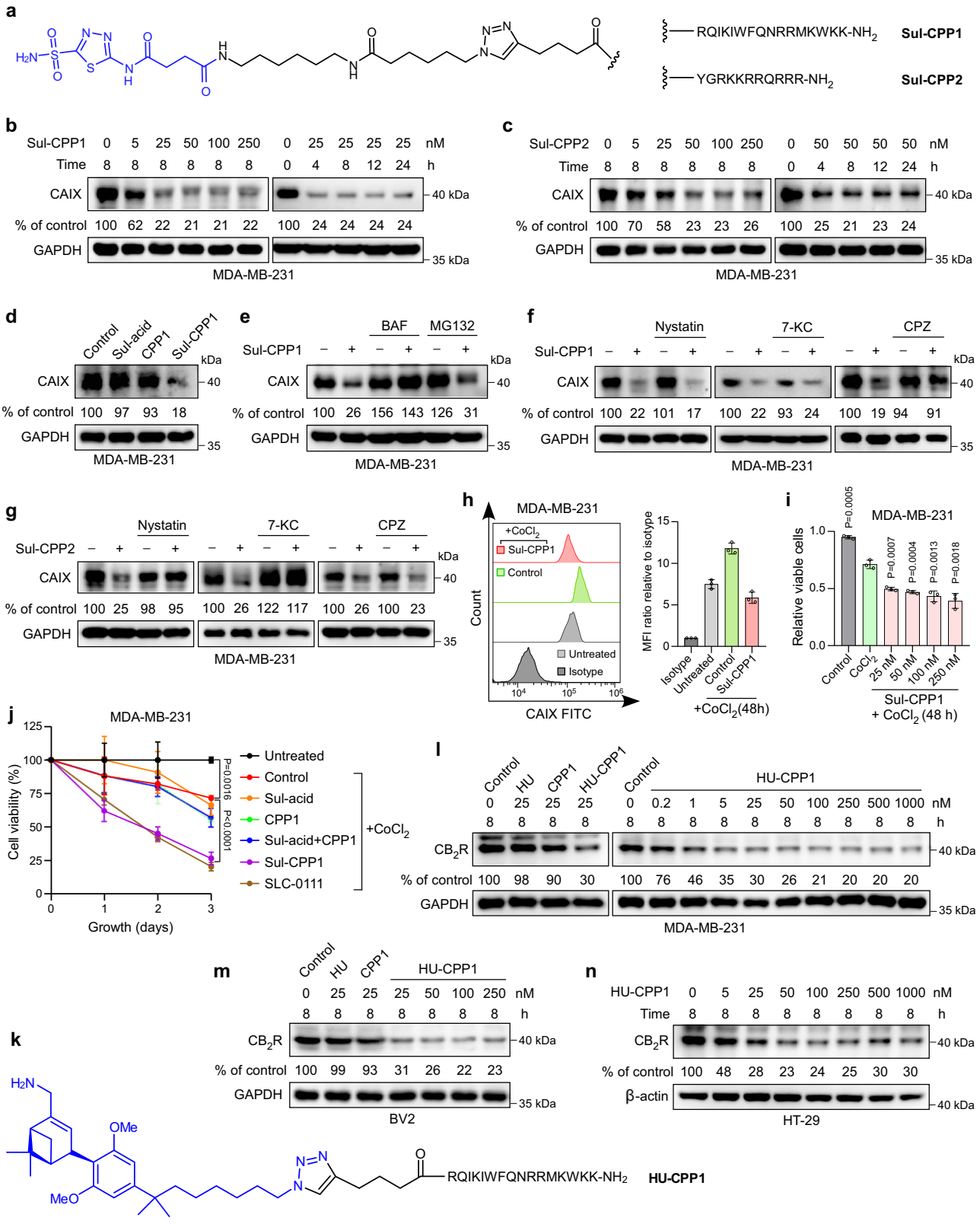

no degradation effect was found in HU- and CPP1- treated groups (Fig. 5l–n and Supplementary Fig. 5d). These results suggest that CPPTACs have the capacity to selectively degrade GPCR family members that share a common architecture of the seven-transmembrane domains. Overall, our findings provide compelling evidence for the broad utility of the CPPTACs platform in effectively degrading diverse plasma membrane proteins.

Discussion

In recent years, there have been advancements in TPD technologies that exploit the endo-lysosome pathway to effectively facilitate the degradation of extracellular and transmembrane proteins. The initial and pivotal step in this process is endocytosis, which entails the creation of endocytic vesicles responsible for transporting the target into the cell and subsequently fusing with lysosomes. As inducers of

Fig. 5 | CPPTACs facilitate the degradation of CAIX and CB_2R. a The structure of Sul-CPP1 and Sul-CPP2. **b**, **c** Western blot analysis of CAIX levels in MDA-MB-231 cells treated with Sul-CPP1 (**b**) or Sul-CPP2 (**c**) at indicated concentration or indicated time. **d** Western blot analysis of CAIX levels in MDA-MB-231 cells treated with Sul-acid, CPP1 or Sul-CPP1 at 25 nM for 8 h. **e** Western blot analysis of CAIX levels in MDA-MB-231 cells treated with Sul-CPP1 (25 nM) for 8 h along with bafilomycin A1 (100 μM) or MG132 (5 μM). **f**, **g** Western blot analysis of the inhibitory effect of Nystatin (50 μM), 7-KC (7-keto-cholesterol, 30 μM) or CPZ (chlorpromazine, 10 μg/mL) on the degradation of CAIX mediated by Sul-CPP1 (**f**) or Sul-CPP2 (**g**). **h** Flow cytometry analysis of the degradation of CAIX in MDA-MB-231 cells mediated by Sul-CPP1 under $CoCl_2$-induced hypoxia conditions. Mean fluorescence intensity of CAIX-FITC relative to the isotype group was quantified ($n = 3$ biological replicates, means ± SD). **i**, **j** The effect of Sul-CPP1 treatment on the survival of MDA-MB-231 cells under $CoCl_2$-induced hypoxia conditions at indicated concentration (**i**) or indicated time (**j**), analyzed by CCK8; $n = 3$ biological replicates. Data represent the mean ± SD. Statistical significance was assessed using two-tailed Student's t-tests or two-way ANOVA. **k** The structure of HU-CPP1. **l**, **m**, **n** Western blot analysis of CB_2R levels in MDA-MB-231 (**l**), BV2 (**m**) or HT-29 cells (**n**) treated with HU-CPP1 for 8 h at indicated concentration. Source data are provided as a Source Data file.

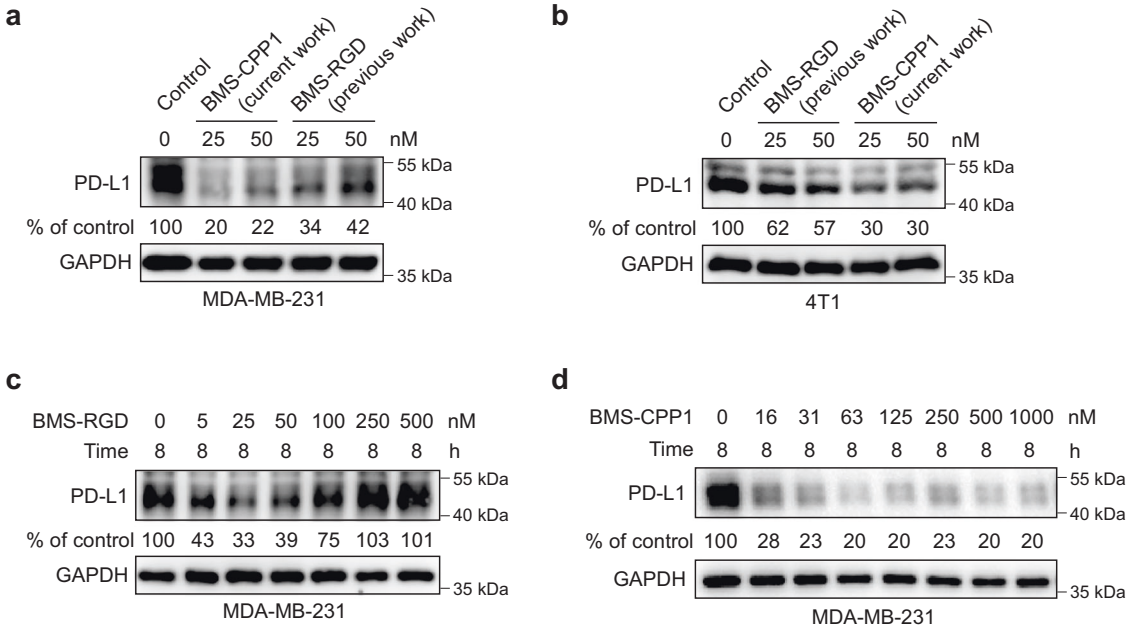

Fig. 6 | Comparison of IFLD- and CPPTAC-mediated degradation of PD-L1. **a**, **b** Western blot analysis of PD-L1 levels in MDA-MB-231 cells (**a**) or 4T1 cells with low expression level of αvβ3 integrin (**b**) treated with BMS-CPP1 or BMS-RGD for 8 h at indicated concentration. **c**, **d** Western blot analysis of PD-L1 levels in MDA-MB-231 cells treated with BMS-RGD (**c**) or BMS-CPP1 (**d**) for 8 h at indicated concentration. Source data are provided as a Source Data file.

endocytosis, CPPs have the capability to initiate various forms of endocytosis, including CME endocytosis, CLIC endocytosis, macropinocytosis, among others. After the formation of endocytic vesicles, CPPs and their cargoes become predominantly confined within endosomes and then transported to lysosomes. Given the remarkable capacity of CPPs to induce endocytosis and direct lysosomal trafficking, we have devised the CPPTACs platform to selectively degrade membrane proteins. Through the conjugation of POI recruiting ligands with various CPPs, CPPTACs capable of targeting both extracellular and cell surface proteins have been fabricated and evaluated. Our findings suggest that the degradation efficacy of CPPTACs is decided by the specific sequences of CPPs employed in the CPPTACs system. Although diverse forms of endocytosis are involved, CPP1 and CPP2, carrying PEN and TAT sequences respectively, exhibited a higher level of effectiveness in promoting targeted protein degradation, compared with CPP3 and CPP4 containing nona-(L/D) arginine sequences. As reported in GlueTAC[16] and SignalTACs[24], the incorporation of a fusion peptide consisting of cell-penetrating and lysosome sorting signals (LSSs) into a nanobody/antibody enhanced the internalization and degradation of the nanobody/antibody-antigen complex. In those studies, LSSs containing tyrosine-based or dileucine-based sorting signals[52] were considered essential for achieving lysosomal localization[34]. In contrast to GlueTACs and SignalTACs, CPPTACs developed in this study demonstrate that various CPPs can induce targeted protein degradation through the endo-lysosomal pathway, without the need of any lysosome sorting sequences.

Unlike other heterobifunctional degraders that require the involvement of specific LTRs, such as the IFLD (integrin-facilitated lysosomal degradation) degraders previously developed by our group[18], CPPTACs demonstrate significant advantages: (1) CPPTACs exhibit greater efficiency compared to IFLD degraders. For instance, CPPTAC (BMS-CPP1) achieves a 75-80% reduction in PD-L1 levels at concentrations of 25-50 nM, whereas the IFLD degrader (BMS-RGD) results in only a 60-65% reduction at the same concentrations (Fig. 6a). (2) CPPTACs have a wider application scope than IFLD degraders. The IFLD strategy's reliance on integrin-mediated endocytosis limits its applicability in cells with low levels of αvβ3 integrin. Conversely, the CPPTACs platform provides a more universally applicable approach for the degradation of plasma membrane proteins across diverse cell types. As demonstrated in Fig. 6b, CPPTAC (BMS-CPP1) efficiently degrades PD-L1 in 4T1 cells, whereas the IFLD degrader (BMS-RGD) exerts only a moderate effect on PD-L1 degradation in the same cells characterized by low αvβ3 integrin expression[53]. (3) CPPTACs have a broader therapeutic window than IFLD degraders. The mechanism of action for a CPPTAC involves the interaction between the small molecule ligand and its target protein, followed by the electrostatic interaction of the CPP sequence with glycans. Given the widespread presence of proteoglycans on the cell surface, which have the potential to interact with CPPTACs, achieving oversaturation of these proteoglycans would require a substantially high concentration of CPPTACs. Consequently, "hook effect" is rarely observed in CPPTAC-mediated degradation of PD-L1 in the concentration range of 16 nM to 1000 nM. This differs from the "target protein-degrader-single LTR"

binding model commonly employed by other heterobifunctional degraders wherein the hook effect arises when an excess of the degrader leads to the predominance of ineffective binary species over ternary complexes. For example, the IFLD degrader (BMS-RGD) shows effective degradation at concentrations ranging from 5 to 50 nM. However, its efficacy diminishes at 100 nM and is entirely lost at concentrations exceeding 250 nM (Fig. 6c, d). (4) In contrast to IFLD degraders, the effectiveness of CPPTACs is largely unaffected by the linker length between the small molecule and the CPP peptide, thereby streamlining the optimization process for CPPTACs. Given these advantages, the CPPTACs approach is widely applicable for the degradation of cell-surface proteins across diverse cell types.

As potentially effective therapeutic strategies, a majority of the engineered degraders that aim at membrane proteins are bifunctional conjugates based on antibodies, nanobodies, or aptamers. It is noteworthy that the CPPTACs developed in this study are composed of CPPs and small-molecule ligands. Due to favorable biocompatibility and high cell membrane permeability of CPPs, numerous CPP-based therapies have progressed to clinical trials and demonstrated promise in the diagnosis and treatment of various diseases. In contrast to antibodies, nanobodies, and aptamers, small molecules generally possess structural stability and immunological tolerability. Besides, small molecules offer advantages such as smaller size, enhanced tissue penetration, and controllable pharmacokinetic properties. Additionally, the accessibility of small-molecule ligands that specifically bind to cell membrane receptors, enzymes, and ion channels offers convenience for the development of CPPTACs. Hence, by harnessing the collective advantages of both CPP and small molecule, CPPTAC represents a reliable approach complementary to degradation technologies relying on antibodies, nanobodies or aptamers.

As demonstrated in this study, CPPTACs are capable of degrading both extracellular and cell surface proteins efficiently through the electrostatic interaction of the CPP sequence with proteoglycans, which are ubiquitously present on the cell surface, rather than via a specific LTR. Our findings indicate that the internalization of RhB-BMS-CPP1 is associated with the expression levels of cell surface PD-L1 at low concentrations (5–100 nM), suggesting that the cell selectivity of a CPPTAC targeting a membrane protein primarily originates from the target itself, but not from proteoglycans. For extracellular proteins, efficient uptake mediated by CPPTAC was observed across a range of cell lines, indicating its potential efficacy in depleting specific disease-related extracellular proteins, such as inflammatory factors (including cytokines and chemokines), monoclonal antibodies (mAbs), and low-density lipoprotein (LDL) from serum. The high abundance of these extracellular proteins poses a challenge for degradation using other TPD technologies that depend on ligand-receptor-mediated endocytosis. It should be noted that the development of CPPTACs as degraders for extracellular and membrane proteins is still in the early stage. The metabolic instability and cytotoxicity inherent to CPPs may adversely affect the in vivo application of CPPTACs. To advance the pharmaceutical application of this strategy, modifications to the CPP motif, such as cyclization or alteration in the peptide sequence, as well as targeted delivery or prodrug technologies, have the potential to enhance the stability of CPPTACs, modify their in vivo biodistribution and metabolic characteristics, and thereby make them more suitable for drug discovery.

In conclusion, the utilization of CPPs as an endocytosis inducer has resulted in the development of a CPPTACs platform, which effectively targets the degradation of cell membrane proteins via the endo-lysosomal pathway. The remarkable efficacy of CPPTACs has been demonstrated in the rapid degradation of various clinically significant membrane proteins, including PD-L1, CAIX, and CB_2R, at nanomolar concentrations. As small molecule-based degraders devoid of the high-dose "hook effect", CPPTACs offer a straightforward, versatile, and highly efficient degradation platform with broad applicability in the fields of chemical biology and drug discovery.

Methods

Animal welfare

All animal experiments were undertaken in accordance with relevant guidelines and regulations and were approved by the Institutional Animal Care and Use Committee (IACUC) of Shenzhen Institutes of Advanced Technology (SIAT), Chinese Academy of Sciences.

General chemistry methods

Analytical RP-HPLC was performed on an Agilent 1260 infinity system equipped with a DAD-UV detector using an Agilent Poroshell 120, EC-C18 column (4.6 mm × 100 mm, 2.7 μm). The RP-HPLC gradient was started at 10% of B (CH_3CN) and then increased to 100% of B over 20 min (A: 0.1% TFA in water) with a flow rate of 0.5 mL/min. The purity of the compounds used for biological study (>95%) was determined by HPLC. Semi-preparative RP-HPLC was performed on the ULTIMAT 3000 instrument (DIONEX). UV absorbance was measured using a photodiode array detector at 220 and 254 nm. The RP-HPLC gradient was started at 10% of B (CH_3CN), and then increased to 100% of B over 20 min (A: 0.1% TFA in water). High-resolution mass spectra were measured with an ABI Q-star Elite.

Full description of the synthetic methods and compound characterization data is included in the Supplementary Information.

Cell lines

A549, HeLa, MDA-MB-231, U87-MG, NCI-H292, NCI-H1975, B16F10, HT-29, 4T1, BV2, BT474, 293 T, HepG2, HUVEC cells, and HeLa cells stably expressing PD-L1 were maintained in DMEM medium (Biological Industries) supplemented with 10% FBS (Invitrogen) and 1% Pen-Strep solution (Biological Industries). NCI-N87 were maintained in RPMI-1640 medium (Biological Industries) supplemented with 10% FBS (Invitrogen) and 1% Pen-Strep solution (Biological Industries). And all of them were cultured in an incubator at 37 °C under 5% CO_2. PD-L1-HA-c-Myc cells (HaLa-HA-PD-L1 cells) stably expressing PD-L1-HA-c-Myc were constructed by infecting HeLa cells with lentivirus containing the full-length human PD-L1-HA-c-Myc gene, identified by western blot and an immunofluorescence microscope. HeLa cells stably expressing HA-tagged PD-L1 and GFP-tagged Gal9 were established by co-infecting the cells with two lentiviruses, respectively carrying the HA-PD-L1 and GFP-Gal9 genes, selected by puromycin and blasticidin, identified by western blot and immunofluorescence microscope.

Fluorescent staining

The cells on the coverslips were washed 2 times with PBS, fixed with 4% formaldehyde solution for 15 min, and rinsed 3 times with PBS (10 mM, pH 7.4) for 5 min each. Following this step, the cell nuclei were stained with DAPI C1005 for 15 min in the dark. The cells were then washed three times with PBS (10 mM, pH 7.4) for 5 min each. The fluorescence images were taken by a Leica STELLARIS 5 confocal fluorescence microscope.

Immunofluorescence

The cells on the coverslips were washed 2 times in PBS, fixed with 4% PFA for 15 min, rinsed 3 times with PBS (10 mM, pH 7.4) for 5 min each. If it is necessary to observe changes of intracellular PD-L1, an additional 0.10% Triton X-100 is required to co-incubate with the cells at room temperature for 15 min. Then, the cells were blocked with 3% BSA for 30 min before being incubated with the indicated primary and secondary antibodies at room temperature for 2 h and 1 h, respectively. Following this step, the cell nuclei were stained with DAPI C1005 for 15 min in dark. The cells were then washed three times with PBS (10 mM, pH 7.4) for 5 min each. The fluorescence images were taken by a Leica STELLARIS 5 confocal fluorescence microscope.

Flow cytometry

The digested cell suspension was centrifuged at 2000 *g* for 3 min at 4 °C, then washed with cold PBS, centrifuged at 2000 g for 3 min at

4 °C. And then, the cells were blocked with 1% BSA+ Fc Receptor Blocker for 15 min before being incubated with the indicated primary and secondary antibodies at 4 °C for 45 min, respectively, and finally resuspended in cold PBS + 1% BSA. Flow cytometry was performed on a CytoFLEX cytometer (Beckman Coulter) using CytExpert software (v2.3.1.22) for data acquisition. Gating was performed on single cells and live cells before acquisition of 10,000 cells. Analysis was performed using FlowJo software (v10.8.0).

Fluorescence analysis of the cellular distribution of CPPs in cells

A549 cells were incubated in a 24-well chambered coverglass slips (Thermo Fisher Scientific) to approximately 40% to 50% confluence. RhB-CPP1-4 were diluted with media to 1 μM. Then the solution was added into the well and the cells were cultured at 37 °C for 8 h. The remaining steps were performed according to the fluorescent staining method described above.

Extracellular protein uptake assay

A549 cells were incubated in a 24-well chambered coverglass slips (Thermo Fisher Scientific) to approximately 40% to 50% confluence. Biotin-CPP1-4 and NAP-650 protein (or NAP-FITC) were diluted to 1 μM and 400 nM in medium, respectively. The mixture was incubated for 30 min to form CPP-tagged NAP-650 (or CPPs-tagged NAP-FITC). The same procedure was used to incubate NAP-650 (or NAP-FITC) with Biotin-Azide and NAP-650 alone. The resulting solution was added to the well, and the cells were cultured at 37 °C for 20 h. When verifying the effect of lysosomal proteolytic activity inhibitor (chloroquine, CQ; bafilomycin A1, BAF) on protein uptake, the cells were co-incubated with CPP-tagged NAP-650 and a solution of CQ (50 μM in medium) or BAF (100 nM in medium) for 12 h. In addition, in order to study the endocytosis pathway, the cells were pre-treated with 50 μM nystatin, 7-KC (30 μM), 10 μg/mL chlorpromazine (CPZ), or 10 μg/mL ethylisopropylamiloride (EIPA) for 1 h before CPP-tagged NAP-650 was added, and the cells were cultured at 37 °C for an additional 8 h. A Trypan Blue quenching assay was performed to eliminate proteins attached to cell membranes. In this assay, following incubation with CPP-tagged NAP-FITC, the cells were treated with 250 μg/mL Trypan Blue on ice for 1 minute. The remaining steps were performed according to the fluorescent staining method, flow cytometry method, or SDS-PAGE gel method described above. For analysis of the efficient uptake of NAP-650 mediated by Biotin-CPP1 in various cell lines, the cells were cultured with the mixture of NAP-650 (100 nM) and Biotin-CPP1 (400 nM) at 37 °C for 6 h and were harvested for flow cytometry analysis as described above.

Co-localization of extracellular protein NAP-650 with the lysosome marker (Lysotracker). A549 cells were incubated in a 24-well chambered coverglass slip to approximately 40% to 50% confluence. The resulting solution of CPP-tagged NAP-650 was added to the well and cultured at 37 °C for 20 h. Then the sample-containing medium was replaced by an equal volume of LysoTracker Green-containing medium, and the cells were further incubated for 1 h. The remaining steps were performed according to the fluorescent staining method described above.

Co-localization of extracellular protein with the early endosome marker (Rab5)

HeLa or A549 cells were incubated in a 24-well chambered coverglass slip to approximately 60% to 70% confluence. Rab5-RFP plasmid was transfected into the cells with PEI transfection reagent. The cells were cultured for 24 h to allow the expression of Rab5-RFP in the early endosomes. Biotin-CPP and NAP-FITC protein were diluted to 1 μM and 400 nM in medium, respectively, and the mixture was incubated for 30 min to form CPP-tagged NAP-FITC. The resulting solution was added to the well, and the cells were cultured at 37 °C for 20 h. The remaining steps were performed according to the fluorescent staining method described above.

CRISPR knockout library screening and data analysis

HeLa cells with a genome-wide CRISPR-Cas9 knockout library were a gift from Yomebio Co. Ltd. The library (Scishare, SSLP011) targeted 19,686 genes with 61,058 unique guide sequences (three sgRNAs/gene). For efficient screening, two replicates of 1.8×10^7 library-infected HeLa cells were incubated with the mixture of NAP-650 (100 nM) and Biotin-CPP1 (500 nM) for 20 h at 37 °C. Cells were harvested and washed three times with PBS containing 2% FBS at 4 °C, and then sorted by FACS using SH800 Cell Sorter (SONY) to select the bottom 5% of the fluorescence distribution in the NAP-650 channel. Sorting was conducted until the whole cells had been processed, which is roughly equivalent to a 300-fold coverage of the library. The collected cells were pelleted and performed genomic DNA extraction. The sgRNA-encoding regions were amplified using One-step CRISPR NGS Library Construction Kit (Yomebio, PK201) according to manufacturer's specifications. The PCR products were sequenced on an Illumina NovaSeq Plus and were analyzed using MaGeCK-VISPR. The enrichment genes in the sorted population were ranked by a positive selection corresponding to the −log (PosScore). The analysis of GO enrichment was performed using MAGeCK-Flute according to −log (FDR).

For further verification, HeLa cells were pre-treated with PEI-B10K (10, 50, 100 nM) or Heparin-Na (0.4, 2, 10, 50 ng/mL) for 30 min before the mixture of NAP-650 (100 nM) and Biotin-CPP (500 nM) was added. Cells were cultured at 37 °C for an additional 20 h and were harvested for flow cytometry analysis as described above.

Fluorescence analysis of Endosome escape

HeLa cells were incubated in a 35 mm glass-bottomed microwell dish (Thermo Fisher Scientific) to approximately 50% to 60% confluence. NF-Cyclic CPP (NF-Cyclic CPP was used as a positive control), NF-CPP1/CPP2, Biotin-CPP1/CPP2, and NAP-NF protein were diluted to 5 μM, 5 μM, 4 μM and 1 μM in medium, respectively. The mixture of Biotin-CPP1/CPP2 and NAP-NF protein was incubated for 30 min to form CPP1/CPP2-tagged NAP-NF. The resulting solution was added to the well, and the cells were cultured at 37 °C for 4 h. The cells were washed 2 times with PBS, the cell nuclei were stained with Hoechst for 5 min in the dark. The cells were then washed with PBS (10 mM, pH 7.4). The fluorescence images were taken by a live cell imaging confocal microscope (Leica STELLARIS 5 confocal fluorescence microscope).

Fluorescence analysis of membrane damage

Hela-PD-L1-bla GFP-Gal9 cells were incubated in a 24-well chambered coverglass slips to approximately 50% to 60% confluence. CPP1, CPP2, BMS-CPP1, BMS-CPP2, and LLOMe (LLOMe was used as a positive control) were diluted to 100 nM, 100 nM, 100 nM, 100 nM, and 1 mM in medium, respectively. The resulting solutions of CPP1, CPP2, BMS-CPP1, and BMS-CPP2 were added to the wells, and the cells were cultured at 37 °C for 4 h. In the positive control group, LLOMe was incubated with the cells at 37 °C for 1 h. The remaining steps were performed according to the fluorescent staining method described above.

Immunofluorescence analysis of membrane protein PD-L1

Hela cells stably expressing PD-L1 (HeLa-HA-PD-L1 cells) were incubated in a 24-well chambered coverglass slip to approximately 40% to 50% confluence. BMS-8, CPP1, BMS-CPP1 and a combination of BMS-8 and CPP1 were diluted with media to 25 nM. Then the solution was added into the well and the cells were cultured at 37 °C for 8 h. The remaining steps were performed according to the immunofluorescence method described above.

The uptake analysis of RhB-BMS-CPP1

HeLa and HeLa-HA-PD-L1 cells were incubated in a 24-well chambered coverglass slip to approximately 40% to 50% confluence. RhB-BMS-

CPP1 was diluted with media to 5 nM, 25 nM, and 100 nM. Then the solution was added into the well and the cells were cultured at 37 °C for 5 h. The remaining steps were performed according to the immunofluorescence method described above.

Western blotting analysis of the PD-L1/CAIX/CB_2R levels

MDA-MB-231, HT-29, BV2, 4T1, or HeLa cells stably expressing PD-L1 were cultured in twelve-well cell plates (JET BIOFIL) to a density of 70–80%. To determine the optimal concentration, BMS-CPP/BMS-RGD/PD-LYSO/Sul-CPP/HU-CPP was diluted to the indicated concentration with DMEM, and co-incubated with the cells for 8 h. For various time intervals, BMS-CPP/Sul-CPP/HU-CPP was diluted to their respective optimal concentrations and introduced to the cells at different time points. In addition, BMS-8, as the control, was treated with the same procedure as above. In order to examine the impact of BMS-CPP1 on PD-L1 degradation in diverse cell types, BMS-8, CPP1, and BMS-CPP1 were diluted to a concentration of 25 nM and incubated with the cells for 8 h. For evaluating BMS-L2-CPP1 and BMS-L3-CPP1 with different linker lengths, they were diluted to 0.04, 0.2, 1, 5, 25, 50, 100, and 250 nM with DMEM, and incubated with the cells for 8 h. When verifying the degradation pathway, bafilomycin A1 (100 nM) was co-incubated with the cells 2 h before BMS-CPP was added, and the cells were cultured at 37 °C for an additional 8 h. In another well, MG132 (5 μM) was added along with BMS-CPP, and the cells were cultured at 37 °C for 8 h. In addition, in order to study the endocytosis pathway, nystatin (50 μM), 7-KC (30 μM), chlorpromazine (CPZ, 10 μg/mL), or ethylisopropyl-amiloride (EIPA, 10 μg/mL) was co-incubated with the cells for 1 h before BMS-CPP was added, and the cells were cultured at 37 °C for an additional 8 h. Then the cells were washed with cold PBS, followed by the addition of SDS lysis buffer (Beyotime, 50-100 μL) containing the protease inhibitor cocktail (1 mM). After centrifugation at 14,000 g for 4 min, the protein samples were boiled for 20 min and then boiled with SDS-PAGE sample loading buffer (5×) for 10 min. The protein samples were separated by 10% sodium dodecyl sulfate polyacrylamide gel (SDS-PAGE gel) for electrophoresis and transferred to a 0.45 μm polyvinylidene fluoride (PVDF) membrane (Millipore). Then, the membranes were blocked with 5% non-fat powdered milk in PBST buffer (PBS + 0.1% Tween-20) for 2 h at room temperature with slight shaking. The membranes were respectively incubated overnight with primary antibodies [PD-L1 antibody, Cell Signaling Technology (CST), rabbit, 1:1000; PD-L1 antibody, Proteintech, mouse, 1:5000; CA9 antibody, Cell Signaling Technology (CST), rabbit, 1:1000; CB_2R antibody, Abcam, rabbit, 1:200; GAPDH antibody, Proteintech, mouse, 1:10000) at 4 °C with slightly shaking. Then, the membranes were washed 3 times (each for 5 min) with PBST buffer. The membranes were incubated with horseradish peroxidase (HRP)-conjugated anti-rabbit IgG antibodies (Proteintech, 1:10000 dilution) and anti-mouse IgG antibodies (CST, 1:5000 dilution) for 1 h at room temperature. At last, the membranes were washed 3 times (each for 5–7 min) with PBST buffer, and the western blot bands were detected by using an electrochemiluminescence (ECL) western blotting substrate (Yeasen Biotechnology, CAT: 36208ES60).

Tumor xenograft mouse models

B16F10 cells (5×10^5) were suspended in 100 μL PBS and injected subcutaneously into the right flank of 6-week-old sterile female C57BL/6J mice (five mice/group, Guangdong Yaokang Biotechnology Co., Ltd). After the tumor size reached 30 mm^3–50 mm^3, the animals were randomly divided into four groups (for each group, $n = 5$). BMS-8 (2 mg/kg), CPP1 (4 mg/kg), the mixture of BMS-8 (1 mg/kg) and CPP1 (2 mg/kg), and BMS-CPP1 (10 mg/kg) dissolved with 1% DMSO/PBS (100 μL) were injected intravenously every two days for six consecutive times. An equal volume of 1% DMSO/PBS was used in the vehicle group. Tumor size and mouse weight were measured before each injection. The tumor volume was calculated as follows: tumor volume = length × width × 1/2width. At Day 16 (16 days after injection of B16F10 cells), the mean tumor volume remained under 1500 mm^3. Notably, only two tumors exceeded this threshold, reaching approximately 1700 mm^3, while all other tumors measured below 1500 mm^3, allowing the continuation of the treatment. At Day 18, we noticed that some tumors had exceeded 2000 mm^3. In accordance with the IACUC guidelines at SIAT, a mouse is deemed to have reached the endpoint and should be euthanized to alleviate suffering when the tumor volume surpasses 2000 mm^3. Additionally, these guidelines stipulate that subcutaneous flank tumors in mice should not exceed a volume range of 2000–3000 mm^3. Consequently, we immediately terminated the animal experiment, collected the tumor samples, and proceeded with weighing and further analysis.

In another experiment, B16F10 cells (2×10^5) were suspended in 100 μL PBS and injected subcutaneously into the right flank of 6-week-old sterile female C57BL/6J mice (five mice/group, Guangdong Yaokang Biotechnology Co., Ltd). After the tumor size reached 30 mm^3-50 mm^3 (L × W × 1/2 W), the animals were randomly divided into three groups (for each group, $n = 5$). BMS-8 (2 mg/kg) and BMS-CPP1 (5 mg/kg) dissolved with 1% DMSO/PBS (100 μL) were peritumorally injected once daily for two consecutive days. An equal volume of 1% DMSO/PBS was used in the vehicle group. The mice were sacrificed after two doses and tumor samples were collected and further analyzed. All the tumor volumes did not exceed 2000 mm^3 during the course of this experiment.

Tumor tissue protein extraction

The tumor tissue was placed in 300 μL RIPA lysis buffer (Beyotime) containing protease inhibitor and phosphatase inhibitors, and 3–5 grinding beads were added. Then the tissue was fully ground with a grinder, and the protein was subsequently lysed by rotating at 4 °C for 30 min, centrifuged at 14,000 g for 10 min, and the supernatant was obtained. Then the protein concentration was determined with the BCA kit (Beyotime), and the protein samples were boiled for 10 min after adding SDS-PAGE sample loading buffer (5×).

Immunohistochemistry of the tumor tissues

The collected melanoma tumors were fixed in 4% paraformaldehyde for 24 h at 4 °C and then embedded in paraffin. Serial sections (4 μm) were prepared for immunohistochemistry (IHC). The paraffin sections were dewaxed in water, placed in xylene for 10 min, twice, then placed in ethanol (100%, 100%, 90%, 80%, 70%, 50%) for 5 min. Then antigen repair was performed, and citric acid repair solution was added and the sections were heated at 95–100 °C for 20 min. After returning to room temperature, the tissue is circled with an immunohistochemical pen to avoid solvent dispersion. Then 3% H_2O_2 was added to inactivate endogenous peroxidase, and the sections were incubated at room temperature for 30 min. The sections were blocked with 5% BSA for 1.5 h. The PD-L1 antibody (Proteintech) was diluted with the primary antibody dilution buffer at 1:2500 and the sections were incubated with the diluted PD-L1 antibody buffer at 4 °C overnight. After washing with PBS for 3 times, the sections were incubated with biotin-conjugated secondary antibody for 30 min, followed by reaction with DAB working solution for color rendering. After color development, the slides were immediately washed with H_2O and counterstained with hematoxylin for 20 s, then they were immediately washed with 1% hydrochloric acid-alcohol and distilled water in turn, and then soaked with 1% ammonia water for 5 min, and washed with distilled water. After dehydration by using an ethanol series and xylene, the immunostained tumor sections were examined by light microscopy, and images were photographed with a microscope camera (Olympus).

Ex vivo fluorescence imaging

B16F10 tumor-bearing C57BL/6J mice were intravenously injected with Cy5.5-CPP1 (4 mg/kg) and Cy5.5-BMS-CPP1 (5 mg/kg). After 6 h, the

organs (heart, liver, spleen, lung, and kidney) and tumors were harvested to photograph. The fluorescence images were acquired using the IVIS Lumina system and analyzed by Living Image software.

Cell survival experiment (CCK8)

MDA-MB-231 cells were inoculated in 96-well plates with approximately 50% to 60% cell density. Sul-acid, CPP1, Sul-CPP1, SLC-0111 and $CoCl_2$ solutions were diluted to 25 nM, 25 nM, 25 nM, 25 nM and 100 μM with DMEM, respectively. The resulting DMEM medium was added into the cell plates, and incubated at 37 °C for 24 h, 48 h, and 72 h. Then the medium was sucked out, and the pre-configured CCK8 solution (10 μL CCK8 solution per 100 μL DMEM) was added to the 96-well plates (100 μL per well). After incubation at 37 °C for 10–30 min, the OD value was determined with a microplate reader at a wavelength of 450 nm. The determination could be finished when until OD value of the control group was between 1 and 1.2; otherwise, the incubation was continued at 37 °C.

Statistics and reproducibility

Blots in Figs. 3a, b, 3e, 5b, c, 5l, S3b–d and S4m–o are representative of three independent experiments with similar results. Blots in Fig. 3c, d, 3h–l, 5d–g, 5m, n, 6a–d, S1e, and S4p are representative of two independent experiments with similar results. Representative images shown in Figs. 1c–e, 1g–i, 3f, g, 4j, S1b, c, S1h, S2c, S2f, S2h, S3e, f, and S5h were derived from at least three independent experiments with similar results. GraphPad Prism 8.0 was used to perform statistical analysis. The data represent the mean ± SD or SEM values of samples obtained from three independent experiments. We performed comparisons between groups using an unpaired two-tailed Student's *t*-test or a two-way ANOVA, as specified in the figure legends. *P* values are indicated in the figures.

Reporting summary

Further information on research design is available in the Nature Portfolio Reporting Summary linked to this article.

Data availability

All raw sequencing data supporting this study have been deposited in the NCBI Sequence Read Archive (SRA) under BioProject accession PRJNA1290636. The dataset spans SRA accessions SRR34512190-SRR34512193. Source data are provided with this paper.

References

1. Yin, H. & Flynn, A. D. Drugging membrane protein interactions. *Annu. Rev. Biomed. Eng.* **18**, 51–76 (2016).
2. Santos, R. et al. A comprehensive map of molecular drug targets. *Nat. Rev. Drug Discov.* **16**, 19–34 (2017).
3. Alabi, S. B. & Crews, C. M. Major advances in targeted protein degradation: PROTACs, LYTACs, and MADTACs. *J. Biol. Chem.* **296**, 100647 (2021).
4. Zhao, L., Zhao, J., Zhong, K., Tong, A. & Jia, D. Targeted protein degradation: mechanisms, strategies and application. *Signal Transduct. Target Ther.* **7**, 113 (2022).
5. Schapira, M., Calabrese, M. F., Bullock, A. N. & Crews, C. M. Targeted protein degradation: expanding the toolbox. *Nat. Rev. Drug Discov.* **18**, 949–963 (2019).
6. Ahn, G., Banik, S. M. & Bertozzi, C. R. Degradation from the outside in: Targeting extracellular and membrane proteins for degradation through the endolysosomal pathway. *Cell Chem. Biol.* **28**, 1072–1080 (2021).
7. Bekes, M., Langley, D. R. & Crews, C. M. PROTAC targeted protein degraders: the past is prologue. *Nat. Rev. Drug Discov.* **21**, 181–200 (2022).
8. Banik, S. M. et al. Lysosome-targeting chimaeras for degradation of extracellular proteins. *Nature* **584**, 291–297 (2020).
9. Ahn, G. et al. LYTACs that engage the asialoglycoprotein receptor for targeted protein degradation. *Nat. Chem. Biol.* **17**, 937–946 (2021).
10. Ahn, G. et al. Elucidating the cellular determinants of targeted membrane protein degradation by lysosome-targeting chimeras. *Science* **382**, eadf6249 (2023).
11. Caianiello, D. F. et al. Bifunctional small molecules that mediate the degradation of extracellular proteins. *Nat. Chem. Biol.* **17**, 947–953 (2021).
12. Marei, H. et al. Antibody targeting of E3 ubiquitin ligases for receptor degradation. *Nature* **610**, 182–189 (2022).
13. Pance, K. et al. Modular cytokine receptor-targeting chimeras for targeted degradation of cell surface and extracellular proteins. *Nat. Biotechnol.* **41**, 273–281 (2023).
14. Cotton, A. D., Nguyen, D. P., Gramespacher, J. A., Seiple, I. B. & Wells, J. A. Development of antibody-based PROTACs for the degradation of the cell-surface immune checkpoint protein PD-L1. *J. Am. Chem. Soc.* **143**, 593–598 (2021).
15. Zhou, Y., Teng, P., Montgomery, N. T., Li, X. & Tang, W. Development of Triantennary N-Acetylgalactosamine conjugates as degraders for extracellular proteins. *ACS Cent. Sci.* **7**, 499–506 (2021).
16. Zhang, H. et al. Covalently Engineered nanobody chimeras for targeted membrane protein degradation. *J. Am. Chem. Soc.* **143**, 16377–16382 (2021).
17. Miao, Y. et al. Bispecific Aptamer chimeras enable targeted protein degradation on cell membranes. *Angew. Chem. Int Ed. Engl.* **60**, 11267–11271 (2021).
18. Zheng, J. et al. Bifunctional compounds as molecular degraders for integrin-facilitated targeted protein degradation. *J. Am. Chem. Soc.* **144**, 21831–21836 (2022).
19. Zhu, C., Wang, W., Wang, Y., Zhang, Y. & Li, J. Dendronized DNA Chimeras Harness scavenger receptors to degrade cell membrane proteins. *Angew. Chem. Int Ed. Engl.* **62**, e202300694 (2023).
20. Wu, Y. et al. Aptamer-LYTACs for targeted degradation of extracellular and membrane proteins. *Angew. Chem. Int Ed. Engl.* **62**, e202218106 (2023).
21. Liu, Y. et al. Aptamer-based targeted protein degradation. *ACS Nano* **17**, 6150–6164 (2023).
22. Wang, K. et al. Nano-LYTACs for degradation of membrane proteins and inhibition of CD24/Siglec-10 signaling pathway. *Adv. Sci.* **10**, e2300288 (2023).
23. Loppinet, E. et al. Targeted lysosomal degradation of secreted and cell surface proteins through the LRP-1 pathway. *J. Am. Chem. Soc.* **145**, 18705–18710 (2023).
24. Yu, J. et al. Harnessing the Lysosomal sorting signals of the cation-independent Mannose-6-phosphate receptor for targeted degradation of membrane proteins. *J. Am. Chem. Soc.* **145**, 19107–19119 (2023).
25. Zhang, B. et al. Insulin-like Growth Factor 2 (IGF2)-Fused Lysosomal targeting chimeras for degradation of extracellular and membrane proteins. *J. Am. Chem. Soc.* **145**, 24272–24283 (2023).
26. Cheng, B. et al. Chemically engineered antibodies for autophagy-based receptor degradation. *Nat. Chem. Biol.* **21**, 855–866 (2025).
27. Casement, R., Bond, A., Craigon, C. & Ciulli, A. Mechanistic and structural features of PROTAC Ternary complexes. *Methods Mol. Biol.* **2365**, 79–113 (2021).
28. Douglass, E. F. Jr., Miller, C. J., Sparer, G., Shapiro, H. & Spiegel, D. A. A comprehensive mathematical model for three-body binding equilibria. *J. Am. Chem. Soc.* **135**, 6092–6099 (2013).
29. Derakhshankhah, H. & Jafari, S. Cell penetrating peptides: A concise review with emphasis on biomedical applications. *Biomed. Pharmacother.* **108**, 1090–1096 (2018).
30. Habault, J. & Poyet, J. L. Recent advances in cell penetrating peptide-based anticancer therapies. *Molecules* **24**, 927 (2019).

31. Xie, J. et al. Cell-penetrating peptides in diagnosis and treatment of human diseases: from preclinical research to clinical application. *Front Pharm.* **11**, 697 (2020).
32. Qian, Z. et al. Discovery and mechanism of highly efficient cyclic cell-penetrating peptides. *Biochemistry* **55**, 2601–2612 (2016).
33. Rennick, J. J., Johnston, A. P. R. & Parton, R. G. Key principles and methods for studying the endocytosis of biological and nanoparticle therapeutics. *Nat. Nanotechnol.* **16**, 266–276 (2021).
34. Han, Y. et al. Protein labeling approach to improve lysosomal targeting and efficacy of antibody–drug conjugates. *Org. Biomol. Chem.* **18**, 3229–3233 (2020).
35. Van Nguyen, T. et al. Cell-penetrating peptide-based non-invasive topical delivery systems. *J. Pharm. Investig.* **48**, 77–87 (2017).
36. Fernández-Delgado M. et al. Study of oligonucleotides access and distribution in human peripheral blood mononuclear cells. *Int. J. Mol. Sci.* **23**, 5839 (2022).
37. Qian, Z., Dougherty, P. G. & Pei, D. Monitoring the cytosolic entry of cell-penetrating peptides using a pH-sensitive fluorophore. *Chem. Commun.* **51**, 2162–2165 (2015).
38. Ruseska, I. & Zimmer, A. Internalization mechanisms of cell-penetrating peptides. *Beilstein J. Nanotechnol.* **11**, 101–123 (2020).
39. Wang, F. et al. Recent progress of cell-penetrating peptides as new carriers for intracellular cargo delivery. *J. Control. Rel.***174**, 126–136 (2014).
40. Zak, K. M. et al. Structural biology of the immune checkpoint Receptor PD-1 and Its ligands PD-L1/PD-L2. *Structure* **25**, 1163–1174 (2017).
41. Chen, T. et al. Peptide-based and small synthetic molecule inhibitors on PD-1/PD-L1 pathway: A new choice for immunotherapy?. *Eur. J. Med Chem.* **161**, 378–398 (2019).
42. Wang, H. et al. HIP1R targets PD-L1 to lysosomal degradation to alter T cell–mediated cytotoxicity. *Nat. Chem. Biol.* **15**, 42–50 (2018).
43. Peng, J. et al. Chemotherapy induces programmed cell death-ligand 1 overexpression via the nuclear factor-κB to foster an immunosuppressive tumor microenvironment in ovarian cancer. *Cancer Res* **75**, 5034–5045 (2015).
44. Thurston, T. L., Wandel, M. P., von Muhlinen, N., Foeglein, A. & Randow, F. Galectin 8 targets damaged vesicles for autophagy to defend cells against bacterial invasion. *Nature* **482**, 414–418 (2012).
45. Queen A., Bhutto H. N., Yousuf M., Syed M. A., Hassan M. I. Carbonic anhydrase IX: A tumor acidification switch in heterogeneity and chemokine regulation. *Semin Cancer Biol.* **86**, 899–913 (2022).
46. Lou, Y. et al. Targeting tumor hypoxia: suppression of breast tumor growth and metastasis by novel carbonic anhydrase IX inhibitors. *Cancer Res.* **71**, 3364–3376 (2011).
47. Asimul Islam K. K. Receptor Chemoprint Derived Pharmacophore Model for Development of CAIX Inhibitors. *J. Carcinogen. Mutagen.* **s8**, 003 (2014).
48. Chu, C. Y. et al. CA IX is upregulated in $CoCl_2$-induced hypoxia and associated with cell invasive potential and a poor prognosis of breast cancer. *Int. J. Oncol.* **48**, 271–280 (2016).
49. McDonald, P. C. et al. A Phase 1 Study of SLC-0111, a novel inhibitor of carbonic anhydrase IX, in patients with advanced solid tumors. *Am. J. Clin. Oncol.* **43**, 484–490 (2020).
50. Hanuš, L. et al. HU-308: a specific agonist for CB2, a peripheral cannabinoid receptor. *Proc. Natl. Acad. Sci.* **96**, 14228–14233 (1999).
51. Sarott, R. C. et al. Development of high-specificity fluorescent probes to enable Cannabinoid Type 2 receptor studies in living cells. *J. Am. Chem. Soc.* **142**, 16953–16964 (2020).
52. Staudt, C., Puissant, E. & Boonen, M. Subcellular trafficking of mammalian lysosomal proteins: an extended view. *Int J. Mol. Sci.* **18**, 47 (2016).
53. Liu, Z., Liu, S., Wang, F., Liu, S. & Chen, X. Noninvasive imaging of tumor integrin expression using (18)F-labeled RGD dimer peptide with PEG (4) linkers. *Eur. J. Nucl. Med. Mol. Imaging* **36**, 1296–1307 (2009).

Acknowledgements

This work was partially supported by Grants 2023YFA0914900 (to L.C.), 2023YFA0915403 (to H.L.), and 2021YFA0910001 (to P.G.) from the National Key Research and Development Program of China, Grants B2401008 (to L.F.) and D2301003 (to L.C.) from Shenzhen Medical Research Funds, Grants JCYJ20220818101404010 (to L.F.) and JCYJ20220818100412028 (to L.F.) from Shenzhen Science and Technology Program, Grants 2023A1515011765 (to L.F.) and 2023B1515040008 (to H.L.) from the Natural Science Foundation of Guangdong Province. We are grateful to Yomebio Co., Ltd. for their help in generating the whole genome CRISPR library for HeLa cells, which are essential for our study. We are grateful to Peking University Shenzhen Graduate School for the assistance with the Mass facility.

Author contributions

L.F., L.C., and H.L. conceived the project and supervised the study. W.H. and Y.L. performed most cell biological, biochemical, and animal experiments. C.C. and J.Z. synthesized and characterized the CPPTACs. Y.Z. participated in the synthesis of CPPTACs. H.S. and M.L. participated in cell culture and immunofluorescence staining. P.G., K.L., X.S., and X.Y. provided special technical support. L.F., W.H., C.C., J.Z., L.C., and H.L. wrote the manuscript.

Competing interests

The authors declare no competing interests.

Additional information

Supplementary information The online version contains supplementary material available at https://doi.org/10.1038/s41467-025-62776-w.

Correspondence and requests for materials should be addressed to Hongchang Li, Liang Chen or Lijing Fang.

Peer review information *Nature Communications* thanks the anonymous reviewer(s) for their contribution to the peer review of this work. A peer review file is available.

Wanyi He[1,7], Congli Chen[1,7], Jiwei Zheng[1,7], Yanyan Li[1,7], Huaihuai Shi[1], Yimin Zhou[1], Meiqing Li[1], Ping Gong[1,2,3,4,5], Ke Liu[1], Ximing Shao[1], Xiaojun Yao[6], Hongchang Li[1,2,3,4,5] ✉, Liang Chen[1,2] ✉ & Lijing Fang[1,2,3,4,5] ✉

[1]Guangdong Key Laboratory of Nanomedicine, CAS-HK Joint Lab of Biomaterials, Shenzhen Institutes of Advanced Technology (SIAT), Chinese Academy of Sciences, Shenzhen 518055, China. [2]University of Chinese Academy of Sciences, Beijing 100049, China. [3]Key Laboratory of Biomedical Imaging Science and System, Chinese Academy of Sciences, Shenzhen 518055, China. [4]State Key Laboratory of Biomedical Imaging Science and System, Shenzhen 518055, China. [5]Sino-Euro Center of Biomedicine and Health, Shenzhen 518024, China. [6]Centre for Artificial Intelligence Driven Drug Discovery, Faculty of Applied Sciences, Macao Polytechnic University, Macao 999078, China. [7]These authors contributed equally: Wanyi He, Congli Chen, Jiwei Zheng, Yanyan Li.
✉e-mail: hc.li@siat.ac.cn; liang.chen@siat.ac.cn; lj.fang@siat.ac.cn